Spatiotemporal Spectroscopy of Fast Excited-State Diffusion in 2D Covalent Organic Framework Thin Films

Laura Spies[1‡], Alexander Biewald[1‡], Laura Fuchs[2], Konrad Merkel[2], Marcello Righetto[3], Zehua Xu[1], Roman Guntermann[1], Rik Hooijer[1], Laura M. Herz[3,4], Frank Ortmann[2], Jenny Schneider[1], Thomas Bein[1*], Achim Hartschuh[1*]

[1]Department of Chemistry and Center for NanoScience (CeNS), University of Munich (LMU), Butenandtstraße 5-13, 81377 Munich, Germany

[2]TUM School of Natural Sciences, Department of Chemistry, Technische Universität München, 85748 Garching, München, Germany

[3]Clarendon Laboratory, University of Oxford, Department of Physics, Oxford OX1 3PU, UK

[4]Institute for Advanced Study, Technische Universität München, Lichtenbergstr. 2a, 85748 Garching, München, Germany

Supporting Information Placeholder

ABSTRACT: Covalent organic frameworks (COFs), crystalline and porous conjugated structures, are of great interest for sustainable energy applications. Organic building blocks in COFs with suitable electronic properties can feature strong optical absorption, whereas the extended crystalline network can establish a band structure enabling long-range coherent transport. This peculiar combination of both molecular and solid-state materials properties makes COFs an interesting platform to study and ultimately utilize photoexcited charge carrier diffusion. Herein, we investigated the charge carrier diffusion in a two-dimensional COF thin film generated through condensation of the building blocks benzodithiophene-dialdehyde **BDT** and *N,N,N',N'*-tetra(4-aminophenyl)benzene-1,4-diamine **W**. We visualized the spatiotemporal evolution of photogenerated excited states in the 2D **WBDT** COF thin film using remote-detected time-resolved PL measurements (RDTR PL). Combined with optical pump terahertz probe (OPTP) studies, we identified two diffusive species dominating the process at different timescales. Initially, short-lived free charge carriers diffuse almost temperature-independently before relaxing into bound states at a rate of 0.7 ps^{-1}. Supported by theoretical simulations, these long-lived bound states were identified as excitons. We directly accessed the lateral exciton diffusion within the oriented and crystalline film, revealing remarkably high diffusion coefficients of 4 $cm^2\ s^{-1}$ (200 K) and diffusion lengths of several hundreds of nanometers and across grain boundaries. Temperature-dependent exciton transport analysis showed contributions from both incoherent *hopping* and coherent *band-like* transport. In the charge transport model developed based on these findings, we discuss the complex impact of order and disorder on charge carrier diffusion within the **WBDT** COF thin film.

INTRODUCTION

The diffusion of excitons is one of the most fundamental processes in semiconducting materials, characterizing their ability to transport energy.[1–3] Large diffusion coefficients D and long diffusion lengths L_D of excited states are crucial for applications in optoelectronic and photocatalytic devices.[4–6] In the quest for novel, more efficient photoactive materials, a long-standing goal has been to link the energy transport ability of a material to its molecular structure, thereby understanding the relationship between electronic properties and structural features.[7,8]

Two-dimensional covalent organic frameworks (2D COFs) are an emerging class of highly ordered, crystalline porous materials built from organic molecules.[9] Due to their structural versatility, they allow for precise control over their optical and electronic features.[10] Through covalent linking of organic building blocks, an extended π-conjugation can be forged, leading to a delocalized electronic system throughout the crystalline and periodic framework, often imparting semiconducting properties to the 2D COF.[11,12] As a result, COFs have been successfully implemented into optoelectronic devices such as light-emitting diodes[13,14], sensors[15] or photovoltaic devices[16–18] and used as photocatalysts[19–21], e.g. for hydrogen evolution and CO_2 reduction. Due to the atomically precise structural control, COFs are highly interesting materials for studying structure-property relationships in photogenerated energy transport.[22–27] So far, excitonic processes in 2D COFs have been studied mostly in colloidal suspensions using transient absorption spectroscopy (TA)[23,25,27] or *via* optical pump terahertz probe spectroscopy (OPTP) on powder pellets and thin films.[28–30] Employing OPTP, effective charge carrier mobilities ranging from 10^{-1} – 10^{0} $cm^2\ V^{-1}\ s^{-1}$ for bulk powders[28,30,31] to exceptionally high values of 10^{2} - 10^{3} $cm^2\ V^{-1}\ s^{-1}$ for thin films[29,32] were determined, while TA studies reported diffusion coefficients in the range of 10^{-5}-

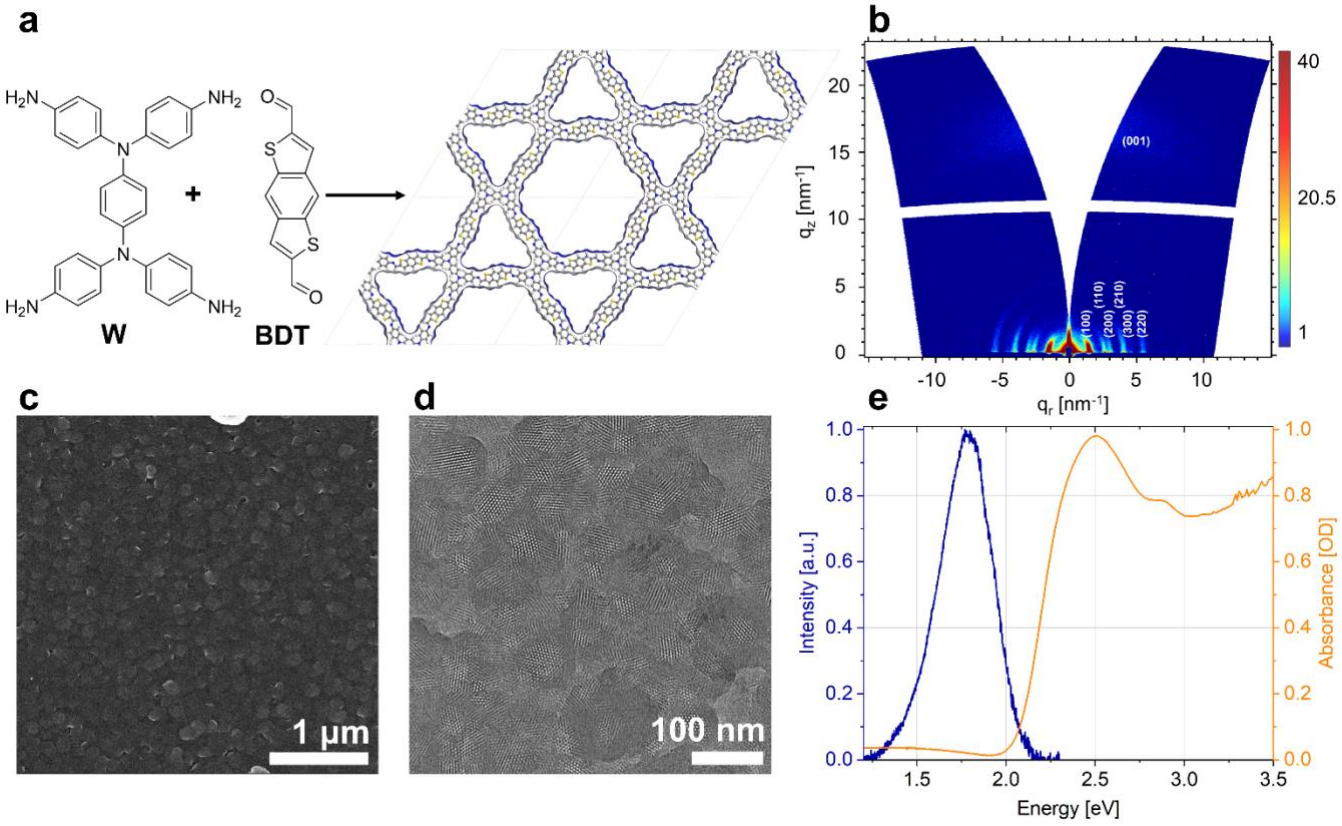

Figure 1. (a) Chemical structure of the two molecular building blocks **W** and **BDT** together with the top view onto a 2×2 supercell, illustrating the Kagomé-like pore structure of the **WBDT** COF. (b) GIWAXS pattern of the **WBDT** thin film on glass with the corresponding *hkl* indices for in-plane (100, 110, 200, 210, 300, 220) and out of plane reflexes (001). (c) SEM top view of the thin film surface. (d) TEM image of the thin film, confirming the preferential crystal orientation within the grains. (d) Normalized steady-state PL and UV-Vis absorption spectra of the **WBDT** thin film.

10^{-2} cm^2 s^{-1} and diffusion lengths of tens of nm for colloidal suspensions of 2D COFs.[25,27] Commonly used techniques to study charge transport in semiconductors include photo[33–36]- and cathodoluminescence[37], terahertz spectroscopy[38,39], microwave conductivity[40,41] or Hall effect measurements[42,43], generally coupled with band structure calculations. However, these methods typically only shed light on particular, often spatially limited aspects of the transport processes and do not provide a full picture of the macroscopic transport properties of emerging semiconducting materials, as these can be strongly affected by structural defects and disorder, interfaces between components, and particularly grain boundaries. Revealing the impact of structural inhomogeneities on energy transport phenomena is key to understanding and developing novel electronic and optoelectronic materials. In recent years, new optical methods imaging the spatiotemporal evolution of photogenerated energy carriers have been developed, providing a more complete picture.[44] The three main spatiotemporal characterization techniques are time-resolved photoluminescence (TRPL),[45] transient scattering (TS)[46] and transient absorption (TA),[47,48] all of which are based on an incipient laser pulse triggering the formation of photogenerated energy carriers and the subsequent imaging of their spatial propagation as a function of time.

In this study, we employ a non-destructive remote-detected time-resolved photoluminescence (RDTR PL) technique to study the temperature-dependent charge carrier diffusion in two-dimensional covalent organic framework (COF) thin films. RDTR PL is a confocal microscopic technique enabling access to local processes occurring on the micrometer length scale. By directly measuring emitted light (PL), single photon detectors can be used, offering high sensitivity of the collected signal. RDTR PL has already been successfully employed to study large-crystal thin films of methylammonium lead iodide (MAPI), a semiconducting material commonly implemented as active layer in perovskite-based solar cells.[45] In the latter case, the extracted diffusion coefficient decreases with increasing temperature, providing crucial information on the dominant charge transport regime in this material. In semiconductors, a description of charge transport is commonly based on two paradigms: coherent *band-like* vs. incoherent *hopping* transport.[49] As seen in MAPI thin films, prevalent *band-like* transport results in a decrease of diffusion coefficient with an increase of temperature, whereas *hopping* transport shows the opposite trend as activation barriers are overcome at higher temperature. Given that COFs are fully organic, crystalline periodic polymers, both types of transport can be relevant for accurately describing the prevailing diffusion regime. The coexistence of *band-like* and *hopping* transport of charge carriers is observed in some organic semiconductors and organic crystals.[50–52] Furthermore, structural and electronic disorder in the system can have a significant and non-intuitive impact on the diffusion of charges or excitons in a semiconductor and must therefore be considered when interpreting experimental data and drafting a charge transport model.[53,54] A comprehensive study of the carrier diffusion and transport mechanisms in COF thin films is still lacking and the powerful RDTR PL technique has not yet been applied to this materials class.

The imine-linked 2D COF thin films studied here comprise the organic building blocks benzodithiophene-dialdehyde **BDT** and *N,N,N',N'*-tetra(4-aminophenyl)benzene-1,4-diamine **W**. This **WBDT** COF, first published by our group in 2020, was chosen for this study because of its significant intrinsic conductivity (1.64×10^{-3} S cm^{-2}) and its tendency to form highly crystalline thin films.[55] We use confocal microscopy to detect remote photoluminescence (RDTR PL), helping us to understand intrinsic properties of the radiative excited state energy transport in this material. We extracted an exceptionally high diffusion coefficient of 4 cm s^{-1} (at 200 K) and diffusion lengths of several hundreds of nm for the lateral transport.

Through thorough analysis of the RDTR PL data in combination with theoretical simulations and optical-pump terahertz probe (OPTP) spectroscopy, we elucidate the diffusion mechanism in **WBDT** thin films involving excitons as the majority energy carriers. For the first time, the use of RDTR PL provides direct access to large-scale diffusion in 2D COFs, allowing for a correlation of the excited state dynamics to the features of the highly crystalline 2D network. Efficient long-range exciton transport can be observed in this **WBDT** COF thin film, with D and L_D values exceeding those of other COFs and organic semiconducting materials by several orders of magnitude.[1,25,27]

RESULTS

In this study, we combined advanced spectroscopic techniques with in-depth theoretical investigations to understand the diffusion dynamics in 2D COF thin films comprised of **BDT** and **W**. Thin films of this fully conjugated COF are highly crystalline and porous, with a Kagomé-like pore structure introduced by the tetra-functionalized **W** node. Both **W** and **BDT** are electron-rich molecules with the former being the more dominant π-donor.

The COF was synthesized according to the literature[55] under solvothermal conditions *via* the acid-catalysed imine condensation of **W** and **BDT** (**Figure 1**a). Thin films were grown on glass or quartz substrates under similar solvothermal conditions as for the bulk material (see section **S3** in the Supporting Information for characterization of the bulk material). The 100, 110, 200, 210, 300, 220 and 001 reflections of the COF crystal lattice are clearly visible in the GIWAXS pattern in **Figure 1**b and appear at identical scattering vectors in the PXRD pattern of the bulk material (**Figure S1**). The intensity of the *hkl* reflections is concentrated in the q_y direction, indicating a predominant orientation of the *a-b* plane of the 2D COF sheets parallel to the substrate with the pores extending vertically from the substrate. Scanning electron micrographs in **Figure 1**c show a dense and uniformly covered thin film with grains of 100 - 200 nm in size and a thickness of ~120 nm, which is further confirmed by atomic force microscopy (AFM) (**Figure S7**). TEM images (**Figure 1**d) confirm the preferential parallel orientation of the COF within the grains. The absence of a defined crystal structure at the grain boundaries implies a disordered character in this region.

Steady-state UV Vis absorption and photoluminescence (PL) spectra are shown in **Figure 1**e. The bright red COF thin film exhibits a maximum absorption at 2.51 eV (494 nm) and an emission peak at 1.78 eV (697 nm) with a full width at half maximum (FWHM) of 0.35 eV. Fitting of the absorption onset using a Tauc plot gives a direct band gap of 2.1 eV (**Figure S6**a). Confocal scanning and hyperspectral imaging of a 10×10 µm^2 section show negligible changes in the normalised intensity, central energy, and spectral width of the PL signal, confirming the homogeneity of the spectral response from the thin film (**Figure S9**).

The calculated band structure of **WBDT** is shown in **Figure 2**. Both the valence and conduction bands exhibit triplet arrangements, typical of structures based on the Kagomé lattice. **WBDT** displays moderate *in-plane* and strong *out-of-plane* band dispersions, which is highest for the valence bands. A Dirac cone is only 0.1 eV away from the top of the valence band. The projection of the states on the atoms of **W** and **BDT** indicates that the frontier electronic levels in the valence band are primarily formed by the atomic orbitals of **W**. The lowest unoccupied bands show a balanced contribution from the atomic orbitals of both fragments.

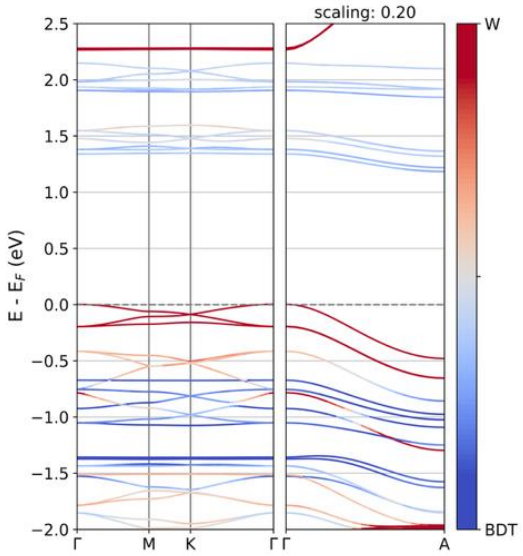

Figure 2. Projected band structure of **WBDT**. Projection on the **W**-based atomic orbitals in red and **BDT** atomic orbitals in blue, calculated using the PBE functional and empirical scissors shift[56] of +0.49 eV to estimate the band gap at Hybrid-DFT (HSE06) level (see section S8 for more details). Darker colors indicate higher weight of states in certain bands on the fragment's atomic orbitals. The distance between Γ and A points has been scaled by 0.2 for illustration purpose.

Time-resolved measurements. In this work, we employ a spatiotemporal characterization technique termed remote detected time-resolved photoluminescence (RDTR PL). This method allows for fully contactless access to intrinsic diffusive transport characteristics of crystalline thin film samples. Herein, a confocal microscope is used for the time-resolved PL measurements, enabling access to the micrometer length scale. The detection segment of the microscope comprises a spectrometer and time-correlated single photon counting (TCSPC) electronics for the temporal resolution. For the spatial resolution, a tiltable mirror is implemented in the back focal plane of the detection part, allowing for scanning around the fixed confocal spot. The aperture of the microscope is defined by the chip of an avalanche photo diode (APD), which, used as a single photon detector, is overfilled by the light emitted from the confocal spot. The studied material is excited with a pulsed laser (510 nm), triggering the formation and subsequent diffusion of photoexcited states from the confocal excitation spot to a remote position, where they recombine whilst emitting a photon. A timestamp is assigned to each of the detected photons, creating a transient. A schematic representation of the methodology is depicted in **Figure 3**a.

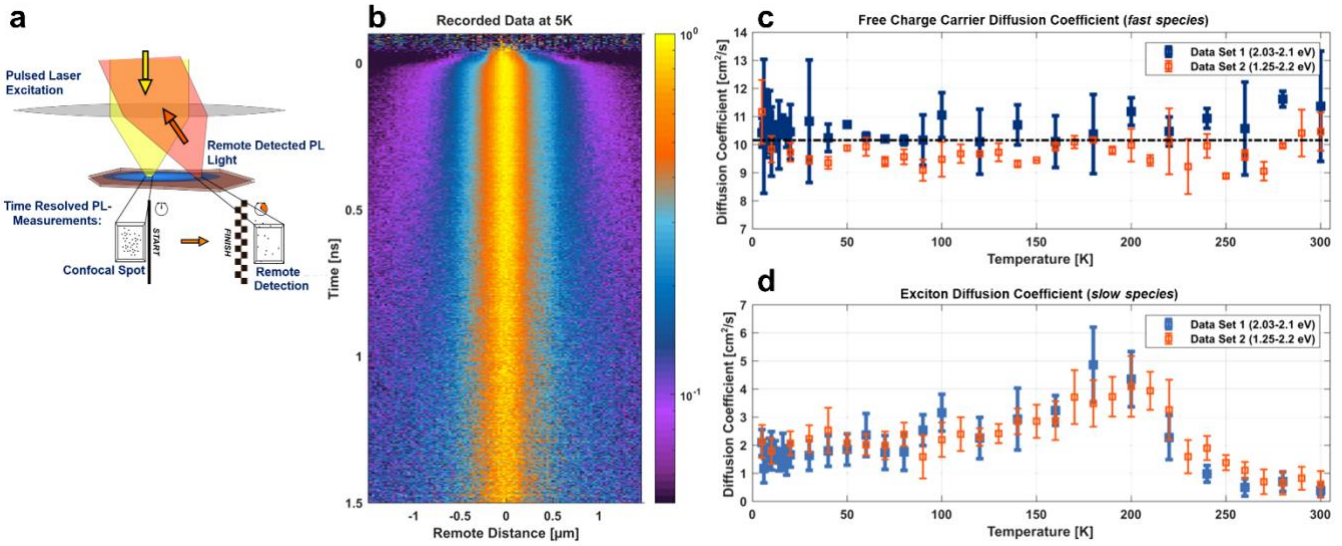

Figure 3. (a) Scheme of the remote-detected time-resolved photoluminescence measurement technique. The pulsed laser (yellow) excites the sample at the confocal spot. Photoluminescence emitted from the confocal spot as well as at remote distances from the confocal spot can be detected (red). The temporal resolution is realized *via* TCSPC. (b) RDTR-PL data at 5K. PL intensity as a function of time (y-axis) and distance (x-axis) from the excitation spot. (c) Temperature independent diffusion coefficient of the free charge carriers (*fast species*) during the first picoseconds after excitation. (d) Exciton (*slow species*) diffusion coefficient as a function of the temperature. For data set 1 and 2, the diffusion coefficient is determined for the blue side of the PL spectrum and for the whole spectrum, respectively.

In the transients obtained via RDTR PL, lateral broadening of the confocal PL spot can be observed (**Figure 3**b). This broadening is caused by two-dimensional diffusion of the excited states in the film. While diffusion in the third dimension (z-direction) is likely to be present, it cannot be accessed through RDTR PL. Since the Rayleigh length of the excitation laser is longer than the thickness of the film, at the laser spot the thin film is excited across its entire thickness (section S5). Therefore, the diffusion extracted from this RDTR PL measurement can be treated as a two-dimensional process. To analyse the spatial broadening of the RDTR PL signal and to determine the temperature-dependent diffusion coefficient $D(T)$, two different methods were used: In method I, a Gaussian peak function is fitted to the RDTR PL data for each time step resulting in the time dependent spatial broadening $\sigma(t)$. As a result of the analysed spatial broadening $\sigma(t)$ of the confocal PL spot, the diffusion coefficient D can be extracted *via* the following relation:

$$\sigma(\mathrm{t}) = \sqrt{2\mathrm{Dt}}$$

Alternatively, in method II the complete time-dependent data set (**Figure 3**b) is fitted using the analytical solution to the 2D diffusion problem to determine D (see section **S5** in SI for details on the analysis and fitting). Due to the finite width of the excitation focus, a Gaussian distribution is assumed as initial condition for both methods. Also, a Gaussian peak function is added with time-independent width attributed to an immobile species in both cases (**Figures S11** and **S12**). All measurements were analysed using both methods for cross-verification and resulted in the same values for the diffusion coefficients within the experimental error (section **S5**). RDTR PL data were collected stepwise across a temperature range from 5 to 300 K.

From the RDTR PL measurements of the **WBDT** film, two diffusion processes at different timescales can be distinguished, visible as two different slopes in the spatial broadening. In the first picoseconds, still within the rise of the PL signal, a fast transport process is observed with diffusion coefficient $D \sim 10$ cm²/s in **Figure 3**c (termed *fast species*). On the longer nanosecond timescale, a slower temperature-dependent diffusion is detected (**Figure 3**d) with significantly lower diffusion coefficient (termed *slow species*). Together with the immobile contribution used in the analysis of the RDTR PL data, the slow and the fast species, at least three different species need to be considered in a comprehensive model description of the excited state dynamics in the studied **WBDT** film.

Immobile species: In general, immobile species can result from defect or disorder-related trap states. Remarkably, the steady-state PL spectrum of the **WBDT** film shows no significant narrowing of the PL band for lower temperatures (**Figure S6**b). This indicates the presence of such lower lying trap states,[54] which would dominate the red side of the PL spectrum. Indeed, when limiting the detection range to the red side of the PL spectrum, no significant spatial broadening of the PL spot in the RDTR PL measurements is observed. In contrast, spatial broadening indicative of excited state diffusion of a *mobile species* can be clearly seen while detecting the blue side of the RDTR PL spectrum (2.03 - 2.10 eV, data set 1 in **Figure 3**c, d). Detecting the whole spectrum (1.25 – 2.20 eV, data set 2 in **Figure 3**c, d) results in the same diffusion coefficient but with a larger fraction of the immobile contribution (0.3 *vs.* 0.2, respectively).

Free charge carriers in WBDT COF: To identify the highly diffusive (*fast*) species observed above (**Figure 3**c) optical pump terahertz probe (OPTP) measurements on the picosecond timescale were conducted. **Figure 4** shows a fluence-independent transient THz signal rising within the first 250 fs upon above band gap excitation (3.1 eV) at three different fluences (100, 80, 60 µJ cm^{-2}). We note that an analogous response has been reported for different types of COFs,[28,30] and can be safely attributed to the presence of free charge carriers in the COF film. Here, OPTP measurements cannot exclude the simultaneous formation of bound exciton states which would give rise to resonances outside of our THz

probing range (0.5-2.5 THz) because of the high exciton binding energies in COFs.[57] From the initial value of the photoconductivity right after excitation, the effective mobility μ of the free ambipolar charge carriers is extracted as $\varphi\mu \sim 0.12 \pm 0.05\ cm^2V^{-1}s^{-1}$, containing the photon-to-free-charge branching ratio φ. The measured

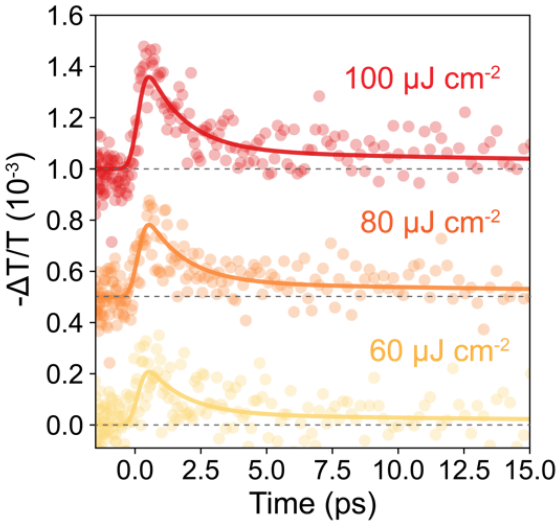

Figure 4. Optical pump terahertz probe measurements. THz photoconductivity transients of **WBDT** COF thin film, measured following a 3.1 eV excitation pulse, for three different excitation fluences (100, 80, 60 µJ/cm^2). For clarity, transients measured at different fluences are vertically shifted and the measurement zero is indicated by the dashed line. Solid lines correspond to a bi-exponential fit to the experimental data.

photoconductivity signal decays by ~ 90% of its initial value with a rate of $k_1 \sim 0.7$ ps^{-1}, thus indicating a minimal remaining fraction of free charge carriers, which subsequently decay more slowly ($k_2 \sim 0.05$ ps^{-1}). We interpret the initial decay as a rapid formation of bound exciton states, whose resonance either lies outside the probing window and / or shows significantly lower mobility. The slower decay of the residual photoconductivity component indicates the presence of alternative decay channels for the surviving free charge-carrier population, such as trapping or bi-molecular recombination. The formation of bound electron-hole pairs as the main species dominating **WBDT** COF's photophysics is further supported by the RDTR PL data, which show significantly longer-lived excited states with lifetimes ranging from ~0.9 to 1.2 ns (**Figure S13**).

Consequently, the initial local broadening of the excitation spot within the first picosecond in the RDTR PL measurements is very likely caused by the diffusion of free charge carriers. Both OPTP and RDTR PL data show that on a fast picosecond timescale, a highly mobile species occurs that rapidly relaxes into bound excitons with lower mobility.

Exciton diffusion in WBDT COF: Exciton (*slow species*) diffusion within the COF thin film is detected by RDTR PL measurements over the nanosecond timescale (**Figure 3**d). To understand and describe the diffusive transport of the excitons, theoretical DFT-based calculations were carried out. Since complete excited state calculations of periodic COF structures are computationally extremely demanding, we opted for a hybrid approach that considers the essential ingredients while being computationally feasible. As illustrated in **Figure 5**, the COF unit cell was disassembled into molecular fragments, six **BDT** and three **W** fragments, respectively. The **W** fragments were H-terminated, while the **BDT** fragments included the imine bonds at the peripheral positions. Time dependent DFT (TDDFT) calculations of the **BDT** and **W** fragments were carried out, including the lowest excitons (at least five per molecule), and provided both localized and delocalized transition densities with variable dipole characteristics of the excited states. The calculated transition dipole moments of **BDT** and **W** fragments have a dominating *in-plane* dipole orientation with moderately large oscillator strengths and asymmetric transition densities (see section **S8** in SI for details on the theoretical calculations). Subsequent re-substitution of the calculated excited states back into the COF structure at the respective fragment position allows for the simulation of exciton interactions between all fragments. These interactions based on the transition charges are dominated by mutually neighbouring pairs, leading to an energy dispersion in the COF lattice. The *in-plane* distance between excitons is much larger than the *out-of-plane* distance (51 Å *vs.* 4 Å), therefore the exciton coupling, although present in the *x-y* plane, is larger in the *z*-direction. For the diffusion coefficient, this anisotropy is partially compensated by the geometry prefactor, *i.e.* the lattice constant, which is larger *in-plane*, enabling the diffusive transport in different directions. The different contributions from both **BDT** and **W** molecules in some of the excited states may well result in a superposition of molecularly localized and partially delocalized states. RDTR PL data confirm the mixing of localized (*immobile species*) and delocalized states as for every time step, the diffusion signal consists of a static component with a constant width and a diffusive component with an increasing spatial width $\sigma(t)$ (**Figure 3**b, **S11** and **S13**).

The overall largest calculated exciton coupling adds up to a moderate value of $\varepsilon \cong 50$ meV. This energy is significantly smaller than most molecular relaxation energies, which suggests that excitons couple more strongly to vibrational modes of the crystal lattice, making them polaronic excitons. We hypothesize that the COF lattice can be deformed in the area surrounding the exciton. The diffusion of the excitons along the 2D COF layers (*in-plane*) is observed in the RDTR PL measurements while the diffusion in *z*-direction across the COF layers will likely be present but cannot be accessed through RDTR PL and is limited by the thickness of the film (~ 120 nm, **Figure S7**).

DISCUSSION OF THE TEMPERATURE-DEPENDENT DIFFUSIVE TRANSPORT

The temperature dependence of the exciton diffusion coefficient contains information on the underlying transport processes in semiconducting materials.[45] Exciton transport in highly ordered, crystalline inorganic semiconductors is typically described as coherent *band-like* transport, where excitons are scattered by phonons and defects.[58,59] For organic polymers, incoherent *hopping* transport is commonly observed, where excited states hop from one electronically favorable state to another, which is described by a hopping rate.[2,58,59] *Band-like* transport is accelerated with decreasing temperature due to reduced phonon scattering while for thermally activated *hopping* transport, the opposite trend is observed. Due to their highly ordered crystalline structure made from molecular building blocks and a delocalized electronic system, COFs can often be described as organic semiconductors, where a combination of both transport phenomena is possible.[11,50,51] As discussed above, the free

charge carriers, dominating the dynamics in the first few picoseconds, diffuse almost temperature-independently with $D \sim 10$ cm^2 s^{-1}. Due to above-band-gap excitation and a laser pulse duration of ≤ 1 ps, the free charge carriers contain excess energy and are thus not in thermal

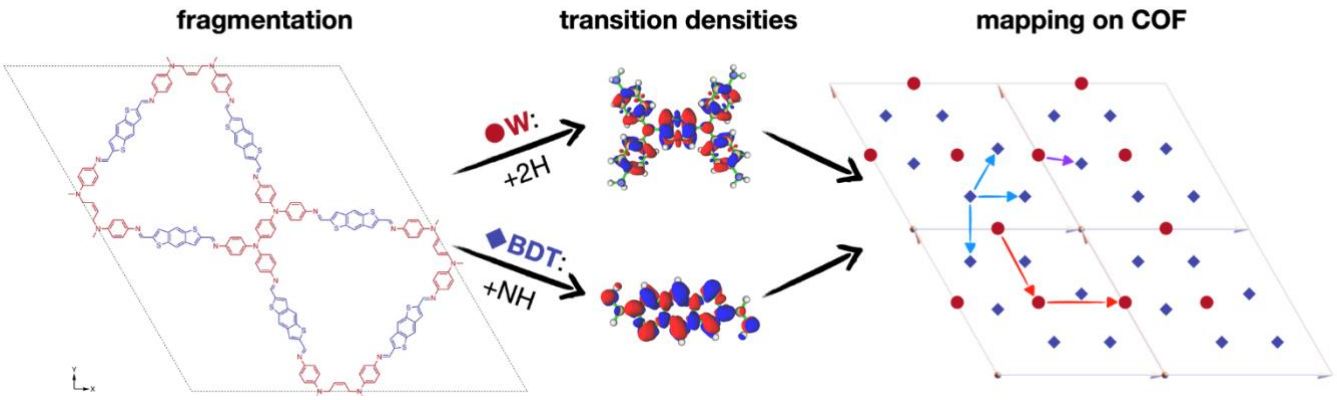

Figure 5. Schematic representation of the hybrid exciton approach: the COF unit cell is divided into molecular fragments of the building blocks **W** and **BDT** (3 and 6 fragments per unit cell, respectively). The transition charges and exciton couplings of these molecular fragments are calculated and the exciton states are placed at the respective positions within the unit cell (red dots indicate centers of mass of **W**, blue diamonds indicate the centers of mass of **BDT**) to carry out exciton interaction and dispersion simulations in-plane and out-of-plane.

equilibrium with the surrounding environment. With the extracted lifetime τ = 1.4 ps from the OPTP measurements, free carriers appear to be converted into bound states before temperature dependent phonon scattering can effectively limit transport. The diffusion length L_D of the free carriers can be estimated using values from the two independent measurements: the lifetime extracted from OPTP and the diffusion coefficient from RDTR PL (see section **S7** in SI for details).[60] A value of $L_D = \sqrt{2D\tau} \approx 50$ nm corresponds roughly to the grain size of the **WBDT** film (**Figure 1**c), which suggests that the carriers can propagate within grains without scattering at grain boundaries.

The combination of the observed and analysed data supports the hypothesis that the mobile free charge carriers relax into a diffusive exciton state within the first picoseconds (**Figure 3**b and **4**) While the initial transient relaxation phase (free charge carriers) is not in the focus of the simulations, diffusion is considered here for the subsequent phase (diffusive excitons). For calculated values of the exciton coupling of $\varepsilon \cong 50$ meV and an estimated reduced reorganization energy of $\Lambda \cong 0.1$ eV,[61] a combination of *band-like* and *hopping* transport in the **WBDT** COF thin film can be expected.[50] This suggests a rather flat or a non-monotonous temperature-dependence of the diffusivity. Also, in this crossover regime *band-like* and *hopping* diffusivities are likely to be comparable in magnitude. Therefore, we apply the simpler hopping ansatz for calculations at room temperature (290 K),[62] A diffusion coefficient of D = 0.2 cm^2 s^{-1} is estimated for the exciton diffusion, which is in good agreement with the experimentally derived range of 0.2 to 0.4 cm^2 s^{-1} at room temperature (**Figure 3**d).

Considering the theoretical model, we tentatively assert that the experimentally observed exciton diffusion coefficient results from a combination of both incoherent (phonon-assisted) *hopping* and coherent *band-like* contributions. Disorder can lead to a complex interplay of these mechanisms, resulting in a non-intuitive temperature dependence, as observed in organic crystals.[53] **Figure 3**d shows that, when the temperature decreases below 300 K, the diffusion coefficient D increases until it reaches a maximum value of 4 cm^2 s^{-1} at approximately 200 K. This suggests that carrier-phonon scattering dominates the temperature dependence of D in this regime, where scattering is enhanced with temperature. This results in a gradual suppression of coherent transport at high temperatures (around room temperature) and an increasing dominance of phonon-assisted incoherent over coherent transport, justifying the use of the hopping model for room temperature calculations. As the temperature lowers, we propose that the transport-relevant phonons start freezing out at 200 K. Consequently, for temperatures below 200 K, an increase in the diffusion coefficient with cooling would be expected for a band regime. However, the opposite is observed, with a gradual decay to 2 cm^2 s^{-1} at the lowest measured temperatures. We propose that the disorder in the COF crystal lattice (including grain boundaries and disorder in the grains) significantly impacts exciton transport at low temperatures, thereby impeding further acceleration of diffusion. Given that incoherent transport is strongly thermally driven, it is suppressed at low temperatures, and we expect the observed diffusion at low temperatures to be mainly coherent and limited by disorder. The remarkably large values observed here suggest the relevance of the third transport direction in the diffusion process, which helps to suppress possible weak/strong localization effects typically seen in lower-dimensional systems. Such lower-dimensional systems are prone to localization, often leading to significantly reduced mobilities in particular at low temperatures which are not observed here.

A schematic model illustrating the excited state diffusion in the **WBDT** COF thin film summarizing the discussion above is shown in **Figure 6**. Free charge carriers with a diffusion length of ~ 50 nm are created within the first picoseconds after excitation and quickly relax into excitons at a rate of $k_1 \sim 0.7$ ps^{-1} (lifetime of 1.4 ps). The excitons with longer lifetimes of up to 1.2 ns are diffusive over several grains (L_D = 200 – 800 nm, **Figure S14**), implying that the excitons in **WBDT** thin films can traverse grain boundaries. In addition to the mobile diffusive species, a non-mobile contribution arising from localized states is visible in the RDTR PL data.

Since RDTR PL measures diffusion over several grains, impurities like defect states, or grain boundaries as well as lattice disorder will all affect the experimentally observed transport behavior. We note that the strongly preferential orientation of the COF layers parallel to the substrate throughout the whole thin film is crucial for efficient lateral diffusion of excitons. In other words, the *z*-axis of each grain is perpendicular to the substrate's plane. To further elucidate

this point, we grew **WBDT** thin films with random crystallite orientation (see section **S6** in

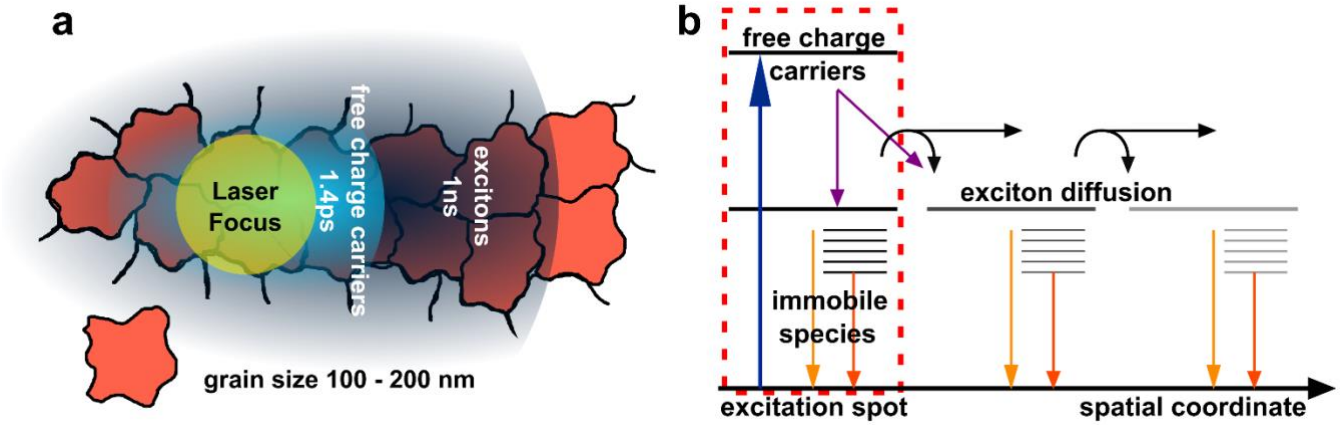

Figure 6. (**a**) Macroscopic and (**b**) energetic representations of excited state diffusion in **WBDT** COF thin films.

SI for details), where the angle between *z*-axis and substrate plane varies for every grain. RDTR PL measurements in those films show substantially reduced exciton diffusion coefficients that decrease with decreasing temperature (**Figure S20**). This change in the diffusion characteristics is due to the anisotropy of the COF crystallites with no extension of the two-dimensional COF structure with the same preferential orientation between the crystallites, hence promoting mainly *hopping*-type transport.

Finally, we compare the derived diffusion coefficients and diffusion lengths for the **WBDT** COF thin films to those reported for other 2D COFs in the literature. To date, excited state diffusion in 2D COFs has been mostly studied using transient absorption spectroscopy of colloidal solutions.[25,27] We note that to the best of our knowledge, the exciton diffusion in the **WBDT** COF films measured *via* RDTR- PL reaches unprecedented values for D and L_D. These values significantly exceed those reported for other COFs and organic semiconducting materials by several orders of magnitude.[1,25,27] We assume that the extended crystallinity of the framework and the uniform orientation of the crystallites in the thin film play a major role in enabling efficient diffusive excited state transport within this **WBDT** COF.

CONCLUSION

In this study we visualized the spatiotemporal evolution of photogenerated excited states in 2D **WBDT** COF thin films using remote detected time-resolved PL measurements. We directly accessed the lateral exciton diffusion within oriented and crystalline thin films of this COF. Remarkably high diffusion coefficients of 4 $cm^2\ s^{-1}$ (at 200 K) and diffusion lengths of several hundreds of nanometers and across grain boundaries were extracted. Furthermore, we analyzed the temperature-dependent exciton transport regime. Phonon-assisted exciton transport prevails above 200 K, while disorder in the system significantly limits the diffusion at temperature below 200 K. Theoretical simulations suggest that the observed diffusion coefficient arises from contributions of both incoherent *hopping* and coherent *band-like* transport. This coexistence of the two regimes was also observed before in organic semiconductors and organic crystals.[50–52] We suggest a dominating coherent transport at low temperatures and a prevailing incoherent transport at room temperature. High crystallinity and preferential orientation of COF thin films allow for a precise definition of the nanoscale structure of the material. Hence, it is evident that energy transport processes are influenced not only by the choice of building units but also significantly by the (dis)order in the molecular framework. With the methodology established here, our work provides a mechanistic understanding of charge and energy transport in macroscopic molecular framework systems, as well as guidance towards enabling efficient transport processes in such materials.

ASSOCIATED CONTENT

Supporting Information

The Supporting Information is available free of charge on the ACS Publications website.
Experimental methods, synthetic procedures, characterization of bulk and film material, information on the analysis and fitting of the spectroscopic data as well as details on the theoretical calculations (PDF).

AUTHOR INFORMATION

Corresponding Author

Achim Hartschuh – Department of Chemistry and Center for Nanoscience (CeNS), Ludwig-Maximilians-Universität (LMU), Munich 81377, Germany; Email: achim.hartschuh@cup.lmu.de

Thomas Bein - Department of Chemistry and Center for Nanoscience (CeNS), Ludwig-Maximilians-Universität (LMU), Munich 81377, Germany; Email: thomas.bein@cup.lmu.de

Present Addresses

Laura Spies - Department of Chemistry and Center for Nanoscience (CeNS), Ludwig-Maximilians-Universität (LMU), Munich 81377, Germany

Alexander Biewald - Department of Chemistry and Center for Nanoscience (CeNS), Ludwig-Maximilians-Universität (LMU), Munich 81377, Germany

Laura Fuchs – TUM School of Natural Sciences, Department of Chemistry, Technische Universität München, Garching Munich 85748, Germany

Konrad Merkel - TUM School of Natural Sciences, Department of Chemistry, Technische Universität München, Garching Munich 85748, Germany

Marcello Righetto – Clarendon Laboratory, University of Oxford, Department of Physics, Oxford OX1 3PU, United Kingdom

Zehua Xu - Department of Chemistry and Center for Nanoscience (CeNS), Ludwig-Maximilians-Universität (LMU), Munich 81377, Germany

Roman Guntermann - Department of Chemistry and Center for Nanoscience (CeNS), Ludwig-Maximilians-Universität (LMU), Munich 81377, Germany

Rik Hooijer - Department of Chemistry and Center for Nanoscience (CeNS), Ludwig-Maximilians-Universität (LMU), Munich 81377, Germany

Laura M. Herz - Clarendon Laboratory, University of Oxford, Department of Physics, Oxford OX1 3PU, United Kingdom and Institute for Advanced Study, Technische Universität München, Lichtenbergstr. 2a, Garching Munich 85748, Germany

Frank Ortmann - TUM School of Natural Sciences, Department of Chemistry, Technische Universität München, Garching Munich 85748, Germany

Jenny Schneider - Department of Chemistry and Center for Nanoscience (CeNS), Ludwig-Maximilians-Universität (LMU), Munich 81377, Germany

Author Contributions

‡ L. S. and A. B. contributed equally. All authors have given approval to the final version of the manuscript.

Notes

The authors declare no competing financial interests.

ACKNOWLEDGMENT

The authors acknowledge funding from the Bavarian Network “Solar Technologies Go Hybrid” and the DFG Excellence Cluster e-conversion (EXC 2089/1-390776260), as well as support through the DFG Priority Program 1928 (COORNETs), grant BE 1042/9-2. The authors thank Dr. Steffen Schmidt for the preparation of SEM images and Dr. Markus Döblinger for performing transmission electron microscopy.

REFERENCES

References

(1) Mikhnenko, O. V.; Blom, P. W. M.; Nguyen, T.-Q. Exciton diffusion in organic semiconductors. *Energy Environ. Sci.* **2015**, *8* (7), 1867–1888.

(2) Morab, S.; Sundaram, M. M.; Pivrikas, A. Review on Charge Carrier Transport in Inorganic and Organic Semiconductors. *Coatings* **2023**, *13* (9), 1657.

(3) Menke, S. M.; Holmes, R. J. Exciton diffusion in organic photovoltaic cells. *Energy Environ. Sci.* **2014**, *7* (2), 499–512.

(4) Tamai, Y.; Ohkita, H.; Benten, H.; Ito, S. Exciton Diffusion in Conjugated Polymers: From Fundamental Understanding to Improvement in Photovoltaic Conversion Efficiency. *J. Phys. Chem. Lett.* **2015**, *6* (17), 3417–3428.

(5) Hodes, G.; Kamat, P. V. Understanding the Implication of Carrier Diffusion Length in Photovoltaic Cells. *J. Phys. Chem. Lett.* **2015**, *6* (20), 4090–4092.

(6) Bisquert, J. Interpretation of electron diffusion coefficient in organic and inorganic semiconductors with broad distributions of states. *Phys. Chem. Chem. Phys.* **2008**, *10* (22), 3175–3194.

(7) Lunt, R. R.; Benziger, J. B.; Forrest, S. R. Relationship between crystalline order and exciton diffusion length in molecular organic semiconductors. *Adv. Mater.* **2010**, *22* (11), 1233–1236.

(8) Rim, S.-B.; Fink, R. F.; Schöneboom, J. C.; Erk, P.; Peumans, P. Effect of molecular packing on the exciton diffusion length in organic solar cells. *Appl. Phys. Lett.* **2007**, *91* (17).

(9) Tan, K. T.; Ghosh, S.; Wang, Z.; Wen, F.; Rodríguez-San-Miguel, D.; Feng, J.; Huang, N.; Wang, W.; Zamora, F.; Feng, X.; Thomas, A.; Jiang, D. Covalent organic frameworks. *Nat. Rev. Methods Primers* **2023**, *3* (1), 1–19.

(10) Keller, N.; Bein, T. Optoelectronic processes in covalent organic frameworks. *Chem. Soc. Rev.* **2021**, *50* (3), 1813–1845.

(11) Huang, W.; Luo, W.; Li, Y. Two-dimensional semiconducting covalent organic frameworks for photocatalytic solar fuel production. *Mater. Today* **2020**, *40*, 160–172.

(12) Blätte, D.; Ortmann, F.; Bein, T. Photons, Excitons, and Electrons in Covalent Organic Frameworks. *J. Am. Chem. Soc.* **2024**.

(13) Ding, H.; Li, J.; Xie, G.; Lin, G.; Chen, R.; Peng, Z.; Yang, C.; Wang, B.; Sun, J.; Wang, C. An AIEgen-based 3D covalent organic framework for white light-emitting diodes. *Nat. Commun.* **2018**, *9* (1), 5234.

(14) Xu, S.; Zhang, Q. Recent progress in covalent organic frameworks as light-emitting materials. *Mater. Today Energy* **2021**, *20*, 100635.

(15) Guo, L.; Yang, L.; Li, M.; Kuang, L.; Song, Y.; Wang, L. Covalent organic frameworks for fluorescent sensing: Recent developments and future challenges. *Coord. Chem. Rev.* **2021**, *440*, 213957.

(16) Calik, M.; Auras, F.; Salonen, L. M.; Bader, K.; Grill, I.; Handloser, M.; Medina, D. D.; Dogru, M.; Löbermann, F.; Trauner, D.; Hartschuh, A.; Bein, T. Extraction of photogenerated electrons and holes from a covalent organic framework integrated heterojunction. *J. Am. Chem. Soc.* **2014**, *136* (51), 17802–17807.

(17) Yildirim, O.; Bonomo, M.; Barbero, N.; Atzori, C.; Civalleri, B.; Bonino, F.; Viscardi, G.; Barolo, C. Application of Metal-Organic Frameworks and Covalent Organic Frameworks as (Photo)Active Material in Hybrid Photovoltaic Technologies. *Energies* **2020**, *13* (21), 5602.

(18) Dogru, M.; Handloser, M.; Auras, F.; Kunz, T.; Medina, D.; Hartschuh, A.; Knochel, P.; Bein, T. A Photoconductive Thienothiophene-Based Covalent Organic Framework Showing Charge Transfer Towards Included Fullerene. *Angew. Chem. Int. Ed.* **2013**, *52* (10), 2920–2924.

(19) Carmo, M. E. G.; Spies, L.; Silva, G. N.; Lopes, O. F.; Bein, T.; Schneider, J.; Patrocinio, A. O. T. From conventional inorganic semiconductors to covalent organic frameworks: advances and opportunities in heterogeneous photocatalytic CO 2 reduction. *J. Mater. Chem. A* **2023**, *11* (26), 13815–13843.

(20) Liu, S.; Wang, M.; He, Y.; Cheng, Q.; Qian, T.; Yan, C. Covalent organic frameworks towards photocatalytic applications: Design principles, achievements, and opportunities. *Coord. Chem. Rev.* **2023**, *475*, 214882.

(21) Bag, S.; Sasmal, H. S.; Chaudhary, S. P.; Dey, K.; Blätte, D.; Guntermann, R.; Zhang, Y.; Položij, M.; Kuc, A.; Shelke, A.; Vijayaraghavan, R. K.; Ajithkumar, T. G.; Bhattacharyya, S.; Heine, T.; Bein, T.; Banerjee, R. Covalent Organic Framework Thin-Film Photodetectors from Solution-Processable Porous Nanospheres. *J. Am. Chem. Soc.* **2023**, *145* (3), 1649–1659.

(22) Streater, D.; Hu, W.; Kelley, M. S.; Yang, S.; Kohlstedt, K. L.; Huang, J. Wavelength-Dependent Excitonic Properties of Covalent Organic Frameworks Explored by Theory and Experiments. *J. Phys. Chem. C* **2023**, *127* (25), 12321–12332.

(23) Jakowetz, A. C.; Hinrichsen, T. F.; Ascherl, L.; Sick, T.; Calik, M.; Auras, F.; Medina, D. D.; Friend, R. H.; Rao, A.; Bein, T. Excited-State Dynamics in Fully Conjugated 2D Covalent Organic Frameworks. *J. Am. Chem. Soc.* **2019**, *141* (29), 11565–11571.

(24) Helweh, W.; Flanders, N. C.; Wang, S.; Phelan, B. T.; Kim, P.; Strauss, M. J.; Li, R. L.; Kelley, M. S.; Kirschner, M. S.; Edwards, D. O.; Spencer, A. P.; Schatz, G. C.; Schaller, R. D.; Dichtel, W. R.; Chen, L. X. Layered structures of assembled imine-linked macrocycles and two-dimensional covalent organic frameworks give rise to prolonged exciton lifetimes. *J. Mater. Chem. C* **2022**, *10* (8), 3015–3026.

(25) Zhang, X.; Geng, K.; Jiang, D.; Scholes, G. D. Exciton Diffusion and Annihilation in an sp2 Carbon-Conjugated Covalent Organic Framework. *J. Am. Chem. Soc.* **2022**, *144* (36), 16423–16432.

(26) Ghosh, S.; Tsutsui, Y.; Kawaguchi, T.; Matsuda, W.; Nagano, S.; Suzuki, K.; Kaji, H.; Seki, S. Band-like Transport of Charge Carriers in Oriented Two-Dimensional Conjugated Covalent Organic Frameworks. *Chem. Mater.* **2022**, *34* (2), 736–745.

(27) Flanders, N. C.; Kirschner, M. S.; Kim, P.; Fauvell, T. J.; Evans, A. M.; Helweh, W.; Spencer, A. P.; Schaller, R. D.; Dichtel, W. R.; Chen, L. X. Large Exciton Diffusion Coefficients in Two-Dimensional Covalent Organic Frameworks with Different Domain Sizes Revealed by Ultrafast Exciton Dynamics. *J. Am. Chem. Soc.* **2020**, *142* (35), 14957–14965.

(28) Wang, M.; Wang, M.; Lin, H.-H.; Ballabio, M.; Zhong, H.; Bonn, M.; Zhou, S.; Heine, T.; Cánovas, E.; Dong, R.; Feng, X. High-Mobility Semiconducting Two-Dimensional Conjugated Covalent Organic Frameworks with p-Type Doping. *J. Am. Chem. Soc.* **2020**, *142* (52), 21622–21627.

(29) Wang, M.; Fu, S.; Petkov, P.; Fu, Y.; Zhang, Z.; Liu, Y.; Ma, J.; Chen, G.; Gali, S. M.; Gao, L.; Lu, Y.; Paasch, S.; Zhong, H.; Steinrück, H.-P.; Cánovas, E.; Brunner, E.; Beljonne, D.; Bonn, M.; Wang, H. I.; Dong, R.; Feng, X. Exceptionally high charge mobility in phthalocyanine-based poly(benzimidazobenzophenanthroline)-ladder-type two-dimensional conjugated polymers. *Nat. Mater.* **2023**, *22* (7), 880–887.

(30) Wang, M.; Ballabio, M.; Wang, M.; Lin, H.-H.; Biswal, B. P.; Han, X.; Paasch, S.; Brunner, E.; Liu, P.; Chen, M.; Bonn, M.; Heine, T.; Zhou, S.; Cánovas, E.; Dong, R.; Feng, X. Unveiling Electronic Properties in Metal-Phthalocyanine-Based Pyrazine-Linked Conjugated Two-Dimensional Covalent Organic Frameworks. *J. Am. Chem. Soc.* **2019**, *141* (42), 16810–16816.

(31) Jin, E.; Fu, S.; Hanayama, H.; Addicoat, M. A.; Wei, W.; Chen, Q.; Graf, R.; Landfester, K.; Bonn, M.; Zhang, K. A. I.; Wang, H. I.; Müllen, K.; Narita, A. A Nanographene-Based Two-Dimensional Covalent Organic Framework as a Stable and Efficient Photocatalyst. *Angewandte Chemie International Edition* **2022**, *61* (5), e202114059.

(32) Fu, S.; Jin, E.; Hanayama, H.; Zheng, W.; Zhang, H.; Di Virgilio, L.; Addicoat, M. A.; Mezger, M.; Narita, A.; Bonn, M.; Müllen, K.; Wang, H. I. Outstanding Charge Mobility by Band Transport in Two-Dimensional Semiconducting Covalent Organic Frameworks. *J. Am. Chem. Soc.* **2022**, *144* (16), 7489–7496.

(33) Banappanavar, G.; Saxena, R.; Bässler, H.; Köhler, A.; Kabra, D. Impact of Photoluminescence Imaging Methodology on Transport Parameters in Semiconductors. *J. Phys. Chem. Lett.* **2024**, *15* (11), 3109–3117.

(34) Kirchartz, T.; Márquez, J. A.; Stolterfoht, M.; Unold, T. Photoluminescence-Based Characterization of Halide Perovskites for Photovoltaics. *Adv. Energy Mater.* **2020**, *10* (26).

(35) Crooker, S. A.; Hollingsworth, J. A.; Tretiak, S.; Klimov, V. I. Spectrally resolved dynamics of energy transfer in quantum-dot assemblies: towards engineered energy flows in artificial materials. *Phys. Rev. Lett.* **2002**, *89* (18), 186802.

(36) Kholmicheva, N.; Moroz, P.; Bastola, E.; Razgoniaeva, N.; Bocanegra, J.; Shaughnessy, M.; Porach, Z.; Khon, D.; Zamkov, M. Mapping the exciton diffusion in semiconductor nanocrystal solids. *ACS Nano* **2015**, *9* (3), 2926–2937.

(37) Coenen, T.; Haegel, N. M. Cathodoluminescence for the 21st century: Learning more from light. *Appl. Phys. Rev.* **2017**, *4* (3).

(38) Johnston, M. B.; Herz, L. M. Hybrid Perovskites for Photovoltaics: Charge-Carrier Recombination, Diffusion, and Radiative Efficiencies. *Acc. Chem. Res.* **2016**, *49* (1), 146–154.

(39) Motti, S. G.; Kober-Czerny, M.; Righetto, M.; Holzhey, P.; Smith, J.; Kraus, H.; Snaith, H. J.; Johnston, M. B.; Herz, L. M. Exciton Formation Dynamics and Band-Like Free Charge-Carrier Transport in 2D Metal Halide Perovskite Semiconductors. *Adv. Funct. Mater.* **2023**, *33* (32).

(40) Kunst, M.; Beck, G. The study of charge carrier kinetics in semiconductors by microwave conductivity measurements. *J. Appl. Phys.* **1986**, *60* (10), 3558–3566.

(41) Hu, Y.; Hutter, E. M.; Rieder, P.; Grill, I.; Hanisch, J.; Aygüler, M. F.; Hufnagel, A. G.; Handloser, M.; Bein, T.; Hartschuh, A.; Tvingstedt, K.; Dyakonov, V.; Baumann, A.; Savenije, T. J.; Petrus, M. L.; Docampo, P. Understanding the Role of Cesium and Rubidium Additives in Perovskite Solar Cells: Trap States, Charge Transport, and Recombination. *Adv. Energy Mater.* **2018**, *8* (16).

(42) Yi, H. T.; Gartstein, Y. N.; Podzorov, V. Charge carrier coherence and Hall effect in organic semiconductors. *Sci. Rep.* **2016**, *6*, 23650.

(43) Karl, N. Charge carrier transport in organic semiconductors. *Synth. Met.* **2003**, *133-134*, 649–657.

(44) Ginsberg, N. S.; Tisdale, W. A. Spatially Resolved Photogenerated Exciton and Charge Transport in Emerging Semiconductors. *Annu. Rev. Phys. Chem.* **2020**, *71*, 1–30.

(45) Biewald, A.; Giesbrecht, N.; Bein, T.; Docampo, P.; Hartschuh, A.; Ciesielski, R. Temperature-Dependent Ambipolar Charge Carrier Mobility in Large-Crystal Hybrid Halide Perovskite Thin Films. *ACS Appl. Mater. Interfaces* **2019**, *11* (23), 20838–20844.

(46) Weaver, H. L.; Went, C. M.; Wong, J.; Jasrasaria, D.; Rabani, E.; Atwater, H. A.; Ginsberg, N. S. Detecting, Distinguishing, and Spatiotemporally Tracking Photogenerated Charge and Heat at the Nanoscale. *ACS Nano* **2023**, *17* (19), 19011–19021.

(47) Cabanillas-Gonzalez, J.; Grancini, G.; Lanzani, G. Pump-probe spectroscopy in organic semiconductors: monitoring fundamental processes of relevance in optoelectronics. *Adv. Mater.* **2011**, *23* (46), 5468–5485.

(48) Grumstrup, E. M.; Gabriel, M. M.; Cating, E. E.; van Goethem, E. M.; Papanikolas, J. M. Pump–probe microscopy: Visualization and spectroscopy of ultrafast dynamics at the nanoscale. *Chem. Phys.* **2015**, *458*, 30–40.

(49) Ortmann, F.; Bechstedt, F.; Hannewald, K. Charge transport in organic crystals: interplay of band transport, hopping and electron–phonon scattering. *New J. Phys.* **2010**, *12* (2), 23011.

(50) Giannini, S.; Carof, A.; Blumberger, J. Crossover from Hopping to Band-Like Charge Transport in an Organic Semiconductor Model: Atomistic Nonadiabatic Molecular Dynamics Simulation. *J. Phys. Chem. Lett.* **2018**, *9* (11), 3116–3123.

(51) Troisi, A. Charge transport in high mobility molecular semiconductors: classical models and new theories. *Chem. Soc. Rev.* **2011**, *40* (5), 2347–2358.

(52) Yavuz, I. Dichotomy between the band and hopping transport in organic crystals: insights from experiments. *Phys. Chem. Chem. Phys.* **2017**, *19* (38), 25819–25828.

(53) Ortmann, F.; Roche, S. Polaron transport in organic crystals: Temperature tuning of disorder effects. *Phys. Rev. B* **2011**, *84* (18).

(54) Ghosh, R.; Paesani, F. Unraveling the effect of defects, domain size, and chemical doping on photophysics and charge transport in covalent organic frameworks. *Chem. Sci.* **2021**, *12* (24), 8373–8384.

(55) Rotter, J. M.; Guntermann, R.; Auth, M.; Mähringer, A.; Sperlich, A.; Dyakonov, V.; Medina, D. D.; Bein, T. Highly conducting Wurster-type twisted covalent organic frameworks. *Chem. Sci.* **2020**, *11* (47), 12843–12853.

(56) Bechstedt, F. *Many-body approach to electronic excitations:Concepts and applications*, Vol. 181; Springer, 2015. DOI: 10.1007/978-3-662-44593-8.

(57) Rahman, M.; Tian, H.; Edvinsson, T. Revisiting the Limiting Factors for Overall Water-Splitting on Organic Photocatalysts. *Angew. Chem. Int. Ed.* **2020**, *59* (38), 16278–16293.

(58) Franchini, C.; Reticcioli, M.; Setvin, M.; Diebold, U. Polarons in materials. *Nat. Rev. Mater.* **2021**, *6* (7), 560–586.

(59) Kittel, C.; McEuen, P. *Introduction to solid state physics*, Global edition; Wiley, 2022.

(60) Wagner, K.; Zipfel, J.; Rosati, R.; Wietek, E.; Ziegler, J. D.; Brem, S.; Perea-Causín, R.; Taniguchi, T.; Watanabe, K.; Glazov, M. M.; Malic, E.; Chernikov, A. Nonclassical Exciton Diffusion in Monolayer WSe2. *Phys. Rev. Lett.* **2021**, *127* (7), 76801.

(61) Vandewal, K.; Benduhn, J.; Schellhammer, K. S.; Vangerven, T.; Rückert, J. E.; Piersimoni, F.; Scholz, R.; Zeika, O.; Fan, Y.; Barlow, S.; Neher, D.; Marder, S. R.; Manca, J.; Spoltore, D.; Cuniberti, G.; Ortmann, F. Absorption Tails of Donor:C60 Blends Provide Insight into Thermally Activated Charge-Transfer Processes and Polaron Relaxation. *J. Am. Chem. Soc.* **2017**, *139* (4), 1699–1704.

(62) Marcus, R. A. Relation between charge transfer absorption and fluorescence spectra and the inverted region. *J. Phys. Chem.* **1989**, *93* (8), 3078–3086.

Table of Contents (ToC)